nature neuroscience

# Asymmetry of *Drosophila* ON and OFF motion detectors enhances real-world velocity estimation

Aljoscha Leonhardt[1,3], Georg Ammer[1,3], Matthias Meier[1], Etienne Serbe[1], Armin Bahl[1,2] & Alexander Borst[1]

**The reliable estimation of motion across varied surroundings represents a survival-critical task for sighted animals. How neural circuits have adapted to the particular demands of natural environments, however, is not well understood. We explored this question in the visual system of *Drosophila melanogaster*. Here, as in many mammalian retinas, motion is computed in parallel streams for brightness increments (ON) and decrements (OFF). When genetically isolated, ON and OFF pathways proved equally capable of accurately matching walking responses to realistic motion. To our surprise, detailed characterization of their functional tuning properties through *in vivo* calcium imaging and electrophysiology revealed stark differences in temporal tuning between ON and OFF channels. We trained an *in silico* motion estimation model on natural scenes and discovered that our optimized detector exhibited differences similar to those of the biological system. Thus, functional ON-OFF asymmetries in fly visual circuitry may reflect ON-OFF asymmetries in natural environments.**



Motion cues resulting from movement through space constitute an important source of information about the external world, supporting course stabilization, navigation or tracking of landmarks[1]. Biological motion detectors have evolved in environments of astounding complexity. Visual landscapes from which animals derive such cues are cluttered and produce rapidly fluctuating signals. Exploiting a priori knowledge about scene features is therefore critical for organisms to reliably extract the spatiotemporal correlations that indicate motion. Basic statistical properties such as the shape of power spectra are known to be conserved between natural scenes[2–4]. Higher order features such as textures, edges or contrast distributions yield additional cues and exhibit consistent statistics across visual environments. Examples of neural adaptation to natural scene statistics abound, operating at various levels of visual processing hierarchies[5–7].

Segregated processing of positive (ON) and negative (OFF) changes in sensory magnitude is a common trait among modalities ranging from olfaction to motion detection in the insect and mammalian visual systems[1,8,9]. Splitting time-varying signals into two streams, covering opposite directions of change, is thought to confer various advantages to sensory circuits. For instance, ON-OFF systems maximize information transfer when resources are constrained[8]. In the case of motion detection, the ON-OFF split may drastically simplify the biophysical implementation of operations such as sign-correct multiplication[10,11].

Luminance distributions in real-world environments are heavily asymmetric with regard to positive and negative contrast[2,12]. Visual systems take this into account: in the mammalian retina, for example, more ganglion cells are dedicated to processing negative than positive spatial contrast, consistent with naturally encountered skewness[13]. Theoretical studies on motion detection have proposed that, in ON-OFF asymmetric environments, higher order correlations carry valuable information about scene motion[14]. Indeed, flies and humans alike appear to be capable of extracting higher order cues[12,15], suggesting that both apply this strategy for motion estimation. However, little is known about the neural mechanism by which either visual system gains access to higher order correlations.

As a result of the availability of powerful genetic tools and extensive connectomic[16,17] as well as functional[18–24] characterizations, knowledge about the neural substrate of *Drosophila* motion detectors has grown exponentially in recent years[9]. Briefly, signals impinging on the photoreceptors are split into two polarity-specific channels, with one processing brightness increases (from L1 to T4 via at least Mi1 and Tm3) and the other processing brightness decreases (from L2, L3 and L4 to T5 via Tm1, Tm2, Tm4 and Tm9). Local ON and OFF motion signals are then extracted on the dendrites of T4 and T5, respectively, in a manner that is well explained by the Hassenstein-Reichardt correlation model[9,11,21]. Large tangential cells in the lobula plate pool these signals and influence behavioral output[1,9,25,26].

Given the ON-OFF asymmetries encountered in natural environments, we set out to determine how the specific features of natural scenes have shaped ON and OFF motion detectors in the fly visual system. In contradistinction to previous studies, we were able to directly assess the behavioral performance of neural pathways by isolating them genetically. We found that asymmetries of natural environments had direct correspondence in tuning asymmetries of the fly motion detection system.

## RESULTS

### ON and OFF motion detectors reliably estimate velocity

Flies react to visual wide-field motion by turning with the environment[1,19,27]. During navigation, this optomotor response stabilizes the animal's course in the face of external perturbations or internal noise.

[1]Max Planck Institute of Neurobiology, Martinsried, Germany. [2]Present address: Department of Molecular and Cell Biology, Harvard University, Cambridge, Massachusetts, USA. [3]These authors contributed equally to this work. Correspondence should be addressed to A.L. (leonhardt@neuro.mpg.de).

Received 19 November 2015; accepted 29 January 2016; published online 29 February 2016; corrected online 7 March 2016 (details online); doi:10.1038/nn.4262

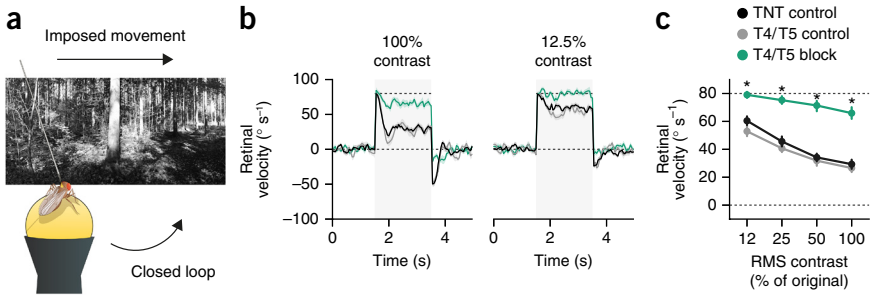


**Figure 1** Flies stabilize their path in naturalistic environments using a combination of ON and OFF motion detectors. (**a**) Illustration of behavioral setup. Tethered flies walk in a virtual closed-loop environment. During certain time periods, their trajectories are perturbed externally. (**b**) Path stabilization under different contrast conditions. Retinal velocity describes environment rotation relative to the fly's eye. During epochs shaded in gray, a constant rotation bias of 80° $s^{-1}$ was added. Upper dashed line indicates imposed velocity. Control flies (TNT control in black, $N = 19$; T4/T5 control in gray, $N = 12$) reduced the imposed retinal velocity effectively whereas T4/T5 block flies (in green, $N = 13$) did not. Left, unmodified image contrast. Right, artificial reduction of root-mean-square (RMS) contrast to 12.5% of initial value. Exact genotypes are listed in **Supplementary Table 1.** (**c**) Quantification of stabilization performance across contrasts. Retinal velocity was averaged between 2 and 3 s. Dashed lines correspond to zero and full correction of the perturbation. Shaded areas around traces and vertical bars signify bootstrapped 68% confidence intervals around the mean. Asterisks indicate significant differences of block flies from both genotype controls after Bonferroni-corrected two-tailed *t* tests (*$P < 0.05$); exact test statistics are reported in **Supplementary Table 2**.

Any deviation from a straight path results in retinal flow that is counteracted by matching direction and, ideally, velocity of perceived drift through locomotion. Responses of behaving fruit flies and wide-field motion-sensitive neurons to simplified motion stimuli such as sinusoidal gratings have been studied extensively[27,28]. Tethered flying flies placed in such artificial environments do indeed correct for externally applied biases[29]. However, flies generally solve this problem in vastly more complex environments. So far, nothing is known about the quantitative extent of their ability to perform path stabilization in naturalistic contexts.

We addressed this question by allowing tethered flies to stabilize their walking trajectories in virtual environments. To cover many possible surroundings, we generated a library of panoramic images spanning the entire visual field of the fly. Randomly selected images were projected onto a virtual cylinder whose orientation was controlled in closed loop through the angular trajectory of flies walking on an air-suspended ball (**Fig. 1a**). In addition, we superimposed fixed-velocity rotations and recorded the relative motion between the fly and its environment. Our approach therefore simulated translation-free walking through a distant visual scene in the presence of external course perturbations. As expected, control flies actively reduced retinal slip speed by rotating in the direction of and with similar velocity as their visual environment (**Fig. 1b**). A combination of neural, motor and setup-intrinsic delays resulted in characteristic over- and undershoots on the order of hundreds of milliseconds, trailing both onset and offset of the motion bias. Notably, control flies rarely achieved a retinal velocity of zero, which would indicate full compensation of the involuntary rotation.

Although combined synaptic silencing of cell types T4 and T5 abolishes behavioral and electrophysiological sensitivity to grating motion[27,30], it is unclear whether naturalistic stimuli can provide additional cues exploited by secondary circuits. When we used Gal4-controlled[31] expression of the light chain of tetanus toxin[32] (TNT) to genetically disrupt synaptic output of all T4 and T5 cells, which are known to implement local motion detection[21,27,30], we discovered a marked impairment of stabilization performance. This was the case across the full range of artificially reduced image contrasts tested (**Fig. 1b**,**c**). The effect did not stem from gross motor defects; the flies' walking speed was at control level (**Supplementary Fig. 1**). Contrast reductions also negatively affected the stabilization ability of control flies. This replicated a previously described property of motion-sensitive lobula plate tangential cells in a behavioral setting: response gain of these cells is diminished for natural images artificially reduced in contrast[33]. In summary, we found that flies actively stabilized their path in complex visual scenes and that T4 and T5 cells were necessary neural elements for this feedback behavior.

Previous work confirmed that T4 and T5 cells are predominantly sensitive to motion defined by luminance increases and decreases, respectively[21]. Full-field motion of naturalistic scenes, especially at large viewing distances and in cluttered environments, creates a rich gamut of both ON and OFF motion. Arrays of ON or OFF detectors may therefore be equally capable of reporting the direction and velocity of realistic global motion. However, nothing is known about the individual contributions of ON and OFF detectors to velocity estimation in such contexts. Moreover, the transformation from stimulus velocity to response strength for all read-outs of the fly motion system is highly sensitive to geometrical features of the stimulus: the fly motion detector is generally not a pure speedometer[1,9]. Even though most gain regimes would eventually lead to stabilization, the optomotor response should ideally match true retinal velocity to correct the fly's course quickly and efficiently[29]. Indeed, tangential cells exhibit a linearized and reliable velocity-response curve when stimulated with natural images as opposed to periodic stimuli such as gratings[33]. We sought to test whether this is reflected by optomotor behavior.

To this end, we assessed *Drosophila's* behavioral ability to track scene velocity in open loop (**Fig. 2a**). Velocity-response curves were stochastically probed by presenting randomly chosen images moving at constant velocities drawn from a Gaussian distribution on each individual trial. Estimation performance was then defined as the linear correlation between environment rotation and average turning response of the fly. A correlation coefficient of $r = 1.0$ indicates a perfectly reliable linear mapping of global motion onto behavioral response across all scenes, as would be required of a functional speedometer. Following visual stimulation, flies responded with robust turning responses that increased until stimulus offset and decayed right after (**Supplementary Fig. 2**). To our surprise, control flies performed the velocity estimation task exceedingly well (**Fig. 2b**). For our image set, individual flies reached correlation coefficients above 0.8 across hundreds of trials. Not all behavioral complexity was captured by the linear model: trials with turning responses close to 0° $s^{-1}$, for instance, were rare (**Fig. 2b**). However, several effects suggested that our simplified measure was indeed valid. First, as anticipated, flies with disrupted T4 and T5 activity exhibited correlation coefficients and response gain close to zero (**Fig. 2c–e**). Second, the correlation coefficients of control flies were heavily decreased by the reduction of image contrast (**Fig. 2d**). This reflected increasing task difficulty at the lower end of the contrast spectrum. Third,

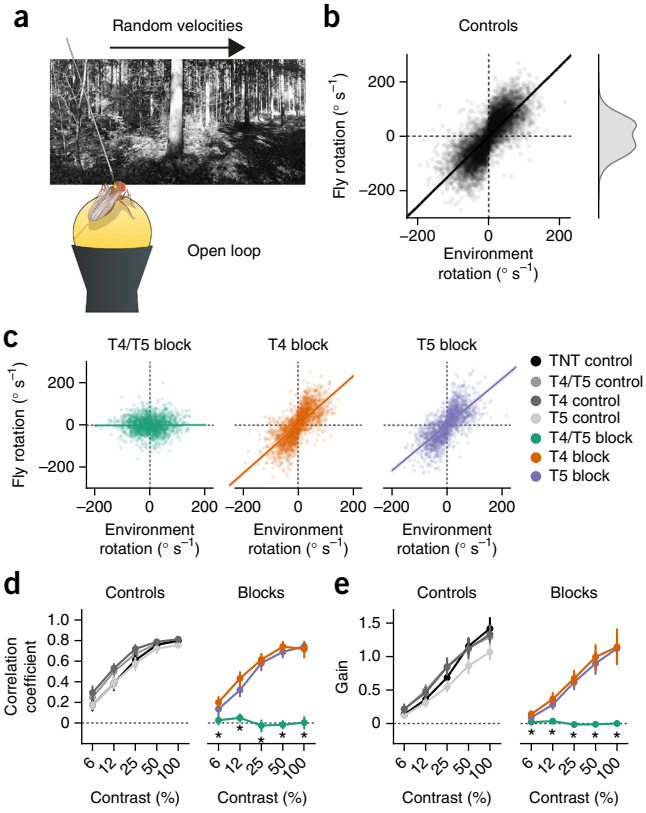


**Figure 2** ON and OFF channels are equally capable of estimating the velocity of natural scenes. (**a**) Sketch of experimental approach. Flies were subjected to a set of natural images rotating at random velocities drawn from a Gaussian distribution (s.d. = 50° $s^{-1}$) in open loop. (**b**) Velocity estimation performance of control flies. Each dot represents the average rotational response for one trial at full contrast. Trials were pooled across flies of all control groups ($n$ = 1,936 trials from $N$ = 13 TNT control flies, $n$ = 1,879/$N$ = 12 for T4/T5 control, $n$ = 2,070/$N$ = 13 for T4 control, $n$ = 1,331/$N$ = 12 for T5 control); the linear fit is for illustrative purposes only. The shaded curve to the right shows a kernel density estimate of rotational responses. (**c**) Velocity estimation performance of block flies, displayed as in **b** ($n$ = 1,755/$N$ = 11 for T4/T5 block, $n$ = 1,976/$N$ = 12 for T4 block, $n$ = 1,778/$N$ = 12 for T5 block). (**d**) Quantification of velocity estimation performance across artificially modified image contrasts. Performance was measured as the Pearson correlation between environment rotation and integrated response. Although T4/T5 block flies were strongly impaired at all contrasts, silencing T4 or T5 individually had no measurable effect on estimation performance. (**e**) Quantification of response gain across contrast range. Gain was measured as the slope of a linear regression model mapping environmental rotation onto rotational response. Vertical bars signify bootstrapped 68% confidence intervals around the mean. Asterisks indicate significant differences for block flies from both Gal4 and UAS controls after Bonferroni-corrected two-tailed $t$ tests (*$P$ < 0.05); exact test statistics are reported in **Supplementary Table 3**.

we once again found a contrast-dependent decrease of response gain as determined by the slope of a linear fit (**Fig. 2e**). It should be noted that these gain values depend on the choice of averaging window. For this reason, and because control systems tend to overcompensate in the absence of feedback, large gain values in open loop do not necessarily entail full compensation in closed loop (**Fig. 1c**).

To determine potentially differential contributions of ON and OFF detectors to velocity estimation in naturalistic contexts, we then silenced only T4 or T5 using TNT. In a previous study using the same lines[21], we found that blocking T4 or T5 led to a strongly reduced ability to detect bright or dark edges, respectively, at both the electrophysiological and behavioral level. In stark contrast to these effects, we found no impairment of velocity estimation for our naturalistic image set. Correlation coefficients for both T4 block and T5 block flies were not substantially different from control groups, even at low contrast levels (**Fig. 2c**,**d** and **Supplementary Fig. 2**). Finally, we alternatively quantified estimation performance as the root-mean-square error of a Bayesian estimator trained on the behavioral data, the results of which supported similar conclusions (**Supplementary Fig. 3**).

Taken together, we found that combined silencing of T4 and T5 completely abolished flies' ability to track the velocity of global motion in naturalistic scenes. Notably, ON and OFF channels appeared to be redundant for this task. Either was sufficient to recapitulate naturalistic behavior.

### Tuning properties of ON and OFF channels are asymmetric

Given that ON and OFF channels seemed equally capable of performing reliable velocity estimation across various visual scenes, it is plausible to assume that they share temporal tuning properties. Previous studies reported comparable temporal frequency optima for sinusoidal gratings[21]. Calcium imaging, however, lacks the temporal resolution required for a precise characterization of pathway kinetics. Moreover, considering the polarity specialization of T4 and T5, we sought to characterize the channels using pure ON or OFF stimuli as opposed to sinusoidal gratings defined equally by brightness increments and decrements.

First, we confirmed that T4 and T5 respond exclusively to bright and dark edges, respectively. The T4 driver line used for imaging in a previous study[21] showed marginal coexpression in T5 cells; the converse applied to the T5 driver line. Our earlier work had revealed minor sensitivity for OFF edges in T4 cells as well as small responses for ON edges in T5 cells, measured in the confines of the lobula plate, where both cell types intermingle. We speculated that this was a result of either Gal4 coexpression or actual physiological crosstalk between ON and OFF circuitry. Moreover, a physiological characterization of T4 input elements suggests that T4 should only be mildly selective for ON motion[24]. To conclusively decide between the alternatives, we performed two-photon calcium imaging using a combined T4 and T5 line in conjunction with the calcium reporter GCaMP6f[34] (**Fig. 3a**). Separation of T4 and T5 signals was then achieved by restricting the region of interest to the cells' dendrites in the medulla or lobula, respectively (**Fig. 3b**). Dendrites showed strong calcium increases following visual edge stimulation that were perfectly polarity specific (**Fig. 3c**,**d**). This allowed us to characterize the temporal tuning properties of T4 and T5 by means of highly time-resolved electrophysiological recordings from downstream cells.

We determined velocity tuning curves for ON and OFF edges moving at speeds spanning two orders of magnitude by recording from the large-field motion-sensitive cells of the horizontal and vertical systems[9,28] in the lobula plate. These cells are the primary recipients of feedforward ON and OFF signals, receiving direct input from T4 and T5 for stimuli moving in preferred direction and indirect inhibitory input via lobula plate interneurons for null direction motion[30,35]. Cells depolarized when stimulated with ON or OFF edge motion along their preferred direction. Unexpectedly, tuning curves as well as general kinetics differed substantially between ON and OFF (**Fig. 3e**). Both channels showed increasing response strength up to a certain velocity, after which responses fell off (**Fig. 3f**). For ON edges, however, this peak was located at approximately 100° $s^{-1}$, whereas OFF responses reached their maximum at edge velocities of ~300° $s^{-1}$. This held true

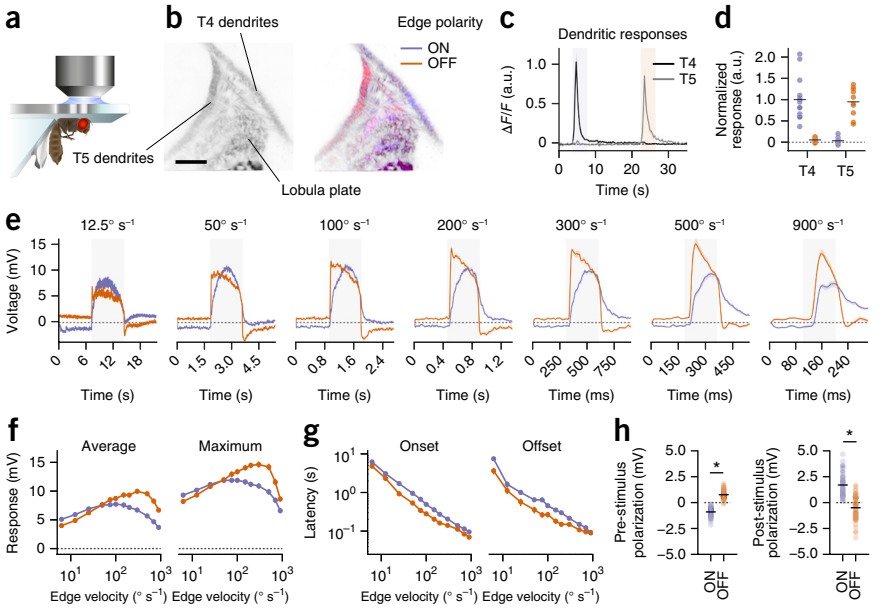


**Figure 3** Physiological characterization of ON and OFF channels reveals tuning asymmetries. (**a**) Schematic of preparation used for two-photon calcium imaging and patch-clamp recordings from lobula plate tangential cells (LPTCs). (**b**) Left, two-photon image of GCaMP6f expression in T4 and T5 cells. Scale bar represents 10 µm. Right, representative T4 and T5 activity during ON (blue) or OFF (red) edge stimulation overlaid onto left-hand image. Activity was confined to T4 or T5 dendrites, depending on edge polarity. (**c**) Relative fluorescence ($\Delta F/F$) across time for regions of interest centered on either T4 (black, $N = 14$) or T5 (gray, $N = 10$) dendrites. (**d**) Quantification of responses as averages over edge presentation period indicated by shaded areas in **c**. (**e**) Average responses of LPTCs for ON and OFF edges moving at a range of velocities in preferred direction. Time axes are scaled differently. Shaded area indicates edge presentation and covers visual field traversal (90°) at the specified velocity. Vertical and horizontal system cells from wild-type flies were pooled ($n = 70$ from $N = 43$ flies). (**f**) Velocity tuning curves for ON and OFF edges based on either average or maximum response during full stimulation period. (**g**) Response kinetics for ON and OFF edges on logarithmic scale. (**h**) Static properties averaged across velocities. Dots represent individual observations and black bars indicate group averages. Vertical bars and shaded areas signify bootstrapped 68% confidence intervals around the mean. Asterisks indicate significant differences between ON and OFF after two-tailed $t$ tests ($^*P < 0.05$). Exact test statistics are reported in **Supplementary Table 4**.

regardless of whether we quantified average or maximum voltage. Moreover, both onset and offset latencies were larger for ON edges than for OFF edges across the full range of velocities tested (**Fig. 3g**). We also observed a constant polarization that closely reflected surround luminance (**Fig. 3h**); for instance, the field illumination preceding the onset of an OFF edge led to steady-state depolarization of the cell, which gave way to hyperpolarization after the dark edge had traveled through the fly's visual field (**Fig. 3e**). In a second set of experiments, we examined whether such differential pre-stimulus polarization could explain the observed ON-OFF asymmetries. Flies were presented with edges starting from an intermediate background luminance that was equal for both polarities (**Supplementary Fig. 4a**). Notably, edge velocity tuning curves were not affected by this alteration, whereas differences in onset kinetics vanished (**Supplementary Fig. 4b,c**). This suggests that luminance adaptation has a strong effect on the dynamics of tangential cell responses, but does not influence temporal tuning.

In summary, we observed strongly differential velocity tuning for ON and OFF pathways, with the former responding maximally to slower velocities than the latter. To determine whether the observed tuning differences are behaviorally relevant, we performed balanced motion experiments on walking flies. Multiple resetting ON and OFF edges distributed across the visual field moved simultaneously in opposite directions over several seconds[19,21,23] (**Fig. 4a**). This was done for a large velocity range and offered a behavioral read-out of the weighting between ON and OFF pathways. Here, a turning tendency of zero implies equal ON and OFF responses. Consistent with electrophysiological results, we found that the balance between ON and OFF responses was clearly modulated by edge velocity (**Fig. 4b**). At low speeds, ON responses dominated the overall turning behavior and control flies continuously rotated in the direction of bright edges (**Fig. 4c**). At higher velocities, this turning tendency was reversed, indicating dominant OFF responses. ON and OFF were only completely in balance at an edge velocity of around 80° $s^{-1}$. To test whether these imbalances also occur at the transient time scales dominating walking behavior, we then shortened the stimulus duration to 500, 250 or 100 ms. These opposing edge pulses produced robust responses whose amplitude diminished with decreasing stimulus length. Notably, all tuning curves had shapes that were comparable to the steady-state condition (**Supplementary Fig. 5**).

We also performed blocking experiments using this assay (**Fig. 4c**). Removing T4 and T5 from the circuit resulted in abolished turning tendencies across all velocities. For individual blocks, we recovered effects whose general direction had been described before[21]: T4 block flies always rotated in the direction of OFF edges and T5 block flies consistently followed motion of ON edges (**Fig. 4b**). Notably, these block effects were most pronounced at different velocities. For T4 block flies, the curve peaked at 160° $s^{-1}$. For T5 block flies, the maximum was found at 80° $s^{-1}$. This roughly confirmed the edge tuning curves from tangential cell recordings (**Fig. 3f**) under the assumption that each individual block was reasonably complete, leaving only one pathway intact. From this, we generated linear predictions for wild-type behavior. *Post hoc* tuning curves were calculated by either subtracting edge tuning curves measured as average voltage or summing the behavioral curves of T4 block and T5 block flies (**Fig. 4d**). Both models successfully predicted response signs and approximate zero crossing of control flies, corroborating the notion that tangential cells combine T4 and T5 signals in an approximately linear regime and then control turning behavior directly.

Despite their comparable performance during naturalistic velocity estimation, the ON and OFF pathways represented by T4 and T5 are tuned to different velocity regimes at both the electrophysiological and behavioral level. We next explored whether this tuning asymmetry is critical for their estimation fidelity.

## Optimized detectors are ON-OFF asymmetric

The *Drosophila* motion detection system is well described by a two-quadrant ON-OFF detector: the combination of two motion detectors, one processing only ON signals akin to the physiological T4 channel and one processing only OFF signals akin to the physiological

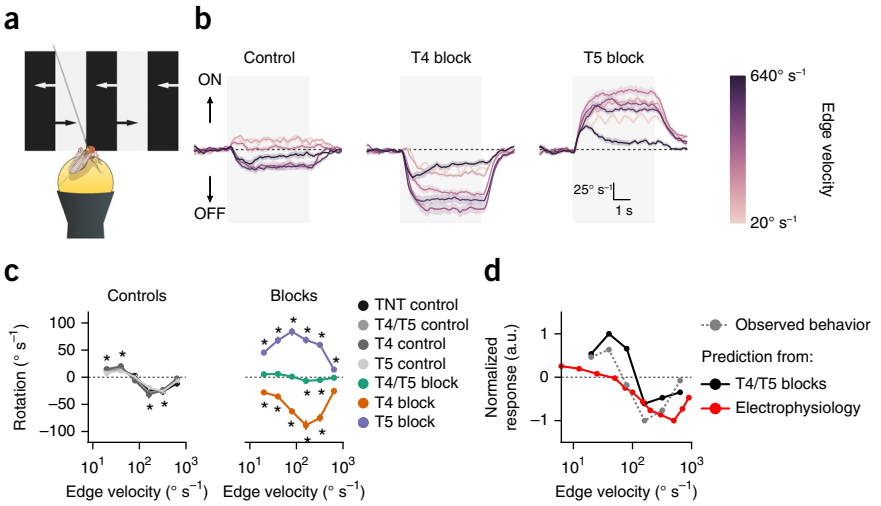


**Figure 4** Asymmetry between ON and OFF channels persists at the behavioral level. (**a**) Schematic drawing of balanced motion stimulus with ON and OFF edges simultaneously moving into opposite directions at various velocities. (**b**) Rotational responses for TNT control flies as well as T4 and T5 block flies. Trace color indicates velocity of edges. Positive responses are syndirectional with ON edge motion; negative responses follow OFF edge motion. Gray-shaded area denotes epoch during which edges were moving. T4 and T5 block flies are consistently biased away from the disrupted polarity. For control flies, the dominant polarity changes with velocity. (**c**) Quantification of turning responses averaged over stimulation period (3 to 7 s; $N = 12$ for TNT control, $N = 12$ for T4/T5 control, $N = 12$ for T4 control, $N = 13$ for T5 control, $N = 12$ for T4/T5 block, $N = 15$ for T4 block, $N = 14$ for T5 block). For controls, asterisks indicate responses that are significantly different from zero ($*P < 0.05$). For block genotypes, asterisks indicate significant differences from both corresponding Gal4 and UAS controls (Bonferroni-corrected $t$ tests, $*P < 0.05$). (**d**) Comparison of observed control tuning curves (gray) with tuning curves linearly predicted from either the sum of behavioral T4 block and T5 block tuning curves (black) or the difference between electrophysiologically determined ON and OFF tuning curves (red; **Fig. 3**). Vertical bars and shaded areas surrounding traces signify bootstrapped 68% confidence intervals around the mean. Exact test statistics are reported in **Supplementary Table 5**.

T5 channel[10]. Each subunit then computes motion according to the well-established Hassenstein-Reichardt correlation model based on the multiplication of differentially filtered, spatially separated signals[11]. Counter-intuitively, such models are capable of explaining complex phenomena such as the reverse-phi effect observed for motion accompanied by contrast reversals[10,19,36]. Critical for this is the inclusion of a weighted tonic signal (DC component) in addition to the high-pass signal modeling processing in lamina monopolar cells. Parameters for the model are generally chosen such that the ON and OFF subunits of the detector remain symmetric[10,19]. Our results concerning edge velocity tuning, however, speak in favor of asymmetric tuning. Moreover, work on natural scenes has repeatedly shown that realistic environments are strongly asymmetric with regard to ON and OFF[2,12,13]. What does an ON-OFF detector look like that is tuned to naturalistic environments?

Various estimation objectives may be prioritized, depending on the given task[29,37]. For this study, we operationalized detector fitness analogously to previous studies[12] and equivalently to our own behavioral experiments as the linear correlation between the velocity of a rigidly translating natural image and time-averaged detector output. Given that Hassenstein-Reichardt detectors directly explain many aspects of fly optomotor behavior[1,9], and considering that flies achieve extremely high correlation values in the corresponding experimental setting (**Fig. 2**), this seemed to be a sensible target for the model. We optimized by exhaustively scanning the parameter space spanned by low-pass filter time constant and DC component of simplified ON and OFF detectors (**Fig. 5a**). This was done in a cross-validated manner. We chose a small set of parameters for optimization in which ON-OFF asymmetries had been observed previously. Our own results on edge tuning (**Fig. 3e**,**f**) indicated that there were large temporal tuning differences between ON and OFF pathways. Physiological characterization of medulla interneurons Mi1 and Tm3 for T4 as well as Tm1 and Tm2 for T5 has revealed distinct differences with regard to the strength of DC signals present at the input of motion detectors[24]. Thus, we looked for combinations of low-pass filter time constants and DC weightings that would maximize velocity estimation performance of isolated ON and OFF detectors for a large set of natural scenes from the van Hateren image database[6]. Velocities were drawn from a Gaussian distribution whose width was based on turning speed distributions determined in our closed-loop experiments. Optimized parameters were modulated in physiologically plausible ranges; all other settings were chosen based on previous modeling work[10] and not tuned for any particular result.

The resulting fitness landscape as a function of low-pass time constant and DC component was smooth and strongly asymmetric with respect to ON and OFF (**Fig. 5b**). Indeed, when we extracted the parameter sets that maximized fitness for independent ON and OFF detectors, we found that optimal settings were ON-OFF asymmetric with respect to both parameters (**Fig. 5c**). Specifically, the best time constants for ON detectors were larger than those achieving maximum correlation for OFF detectors. The best DC weights had higher values for ON detectors than for OFF detectors and opposite signs (**Fig. 5c**).

To ascertain whether parameter asymmetry improved velocity estimation over that achieved by symmetric models, we compared equally weighted combinations of independently optimized ON and OFF detectors to optimized detectors that were constrained to be symmetric. The cross-validated performance improvement was small but significant ($t(98) = 4.08$, $P < 0.001$), suggesting that detector asymmetry is an advantageous strategy (**Fig. 5d**). The differences between ON and OFF parameters of optimal asymmetric models were substantial (**Fig. 5e**). We therefore looked for functional disparities between the average optimized models. Simulated temporal frequency tuning curves for sinusoidal gratings were highly similar, with slightly shifted response optima (**Fig. 5f**). The asymmetric and the symmetric model also produced comparable output for a dynamically moving grating (**Fig. 5g**). When we simulated edge velocity tuning curves as we had measured experimentally (**Figs. 3** and **4**), the symmetric model exhibited identical tuning for ON and OFF edges, as was expected from identical temporal parameters. Our asymmetric model, however, correctly replicated the shift between optima for ON and OFF edges with the detector being tuned to higher OFF than ON edge velocities (**Fig. 5h**). In addition, the asymmetric model predicted a difference in overall strength between ON and

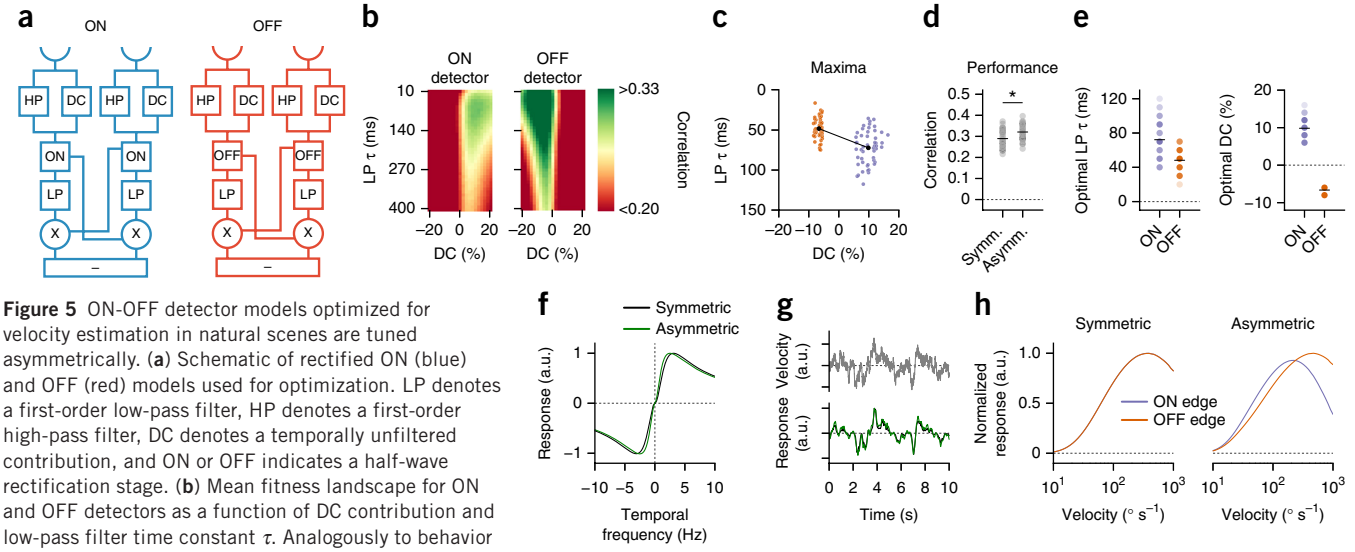


**Figure 5** ON-OFF detector models optimized for velocity estimation in natural scenes are tuned asymmetrically. (**a**) Schematic of rectified ON (blue) and OFF (red) models used for optimization. LP denotes a first-order low-pass filter, HP denotes a first-order high-pass filter, DC denotes a temporally unfiltered contribution, and ON or OFF indicates a half-wave rectification stage. (**b**) Mean fitness landscape for ON and OFF detectors as a function of DC contribution and low-pass filter time constant $\tau$. Analogously to behavior (**Fig. 2d**), estimation performance was measured as the Pearson correlation between input velocity and average detector output. (**c**) Distribution of optimized parameters. Each dot represents the best parameter set found for either ON (blue) or OFF (red) detectors on a given training image set ($N = 50$ folds; points are jittered for clarity). Black dots mark the center of the ON and OFF parameter clouds. (**d**) Cross-validated performance of detectors. Optimal ON and OFF detectors are linearly combined (asymmetric detectors), tested on images not seen during training and compared with ON-OFF detectors optimized under the additional constraint of ON-OFF symmetry. The difference was significant after a two-tailed $t$ test ($N = 50/50$, $t(98) = 4.08$, $^*P < 0.001$). (**e**) Comparison of parameters for asymmetric detectors from **c**. (**f**) Temporal tuning of optimized symmetric and asymmetric detector. (**g**) Responses of optimized symmetric and asymmetric detector to a sinusoidal grating drifting with Gaussian velocity profile. (**h**) Simulated ON and OFF edge velocity tuning curves (with peaks for the asymmetric model at 230 and 480° $s^{-1}$, respectively). Dots represent individual results and black bars indicate group averages.

OFF edge responses (**Fig. 3f**) even though subunits were summed at equal gain. The modeled edge optima occurred at higher velocities than those we had determined experimentally. As optimized parameters for the detectors depended on the s.d. of the distribution from which test velocities were drawn, their absolute scale was somewhat arbitrary; conditional on behavioral state, turning speed distributions may differ substantially. The direction of the asymmetry, however, was consistent with experimental findings.

We then determined natural image features necessary for asymmetries to appear in tuned ON-OFF detectors. To this end, we repeated the optimization procedure for image sets in which we had manipulated specific statistical properties. First, for the unaltered set, the best asymmetric ON and OFF detectors showed large differences for both low-pass time constant, as well as absolute DC level (**Fig. 6a**). Second, we randomized the phase structure of every image, thereby removing all higher level features such as textures or edges, as well as making scenes largely ON-OFF symmetric[13], while retaining the typical power spectrum of natural scenes. Here, the asymmetry of time constants disappeared (**Fig. 6b**). Third, we artificially reinstated the natural luminance distribution in phase-randomized images (**Fig. 6c**). This manipulation rescued the time constant asymmetry, suggesting that a skewed luminance distribution is the critical constraint forcing filter

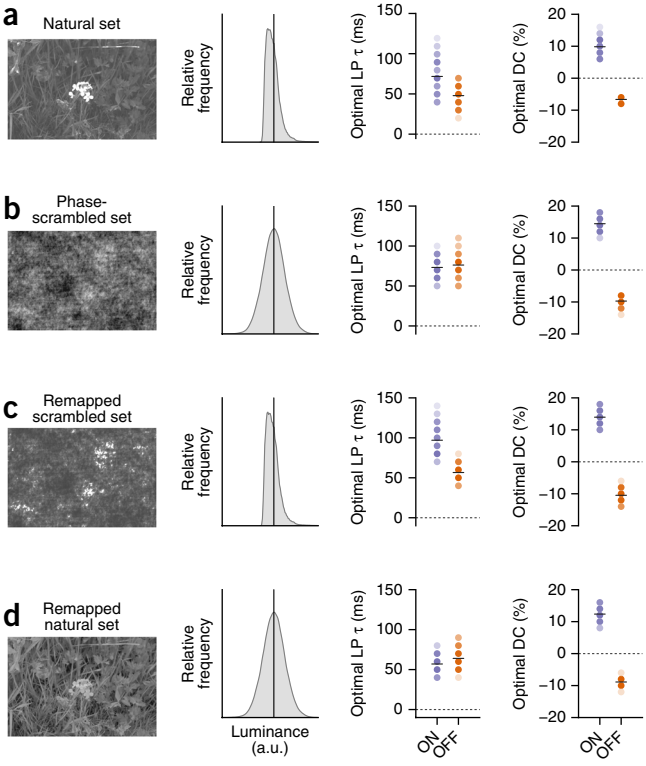


**Figure 6** Luminance asymmetry in natural scenes is critically responsible for asymmetry of ON-OFF parameters in optimized motion detector. (**a**–**d**) Left, example picture from image set used for optimization. Middle, kernel density estimate of pixel luminance distribution for example picture. The vertical line indicates average image luminance. Right-hand panels, optimized parameters for ON (blue) and OFF (red) detector trained on corresponding image set. (**a**) Unmodified image set used for earlier optimizations (**Fig. 5**). (**b**) Phase-scrambled image set in which the phase structure of each image was replaced by that of a random image, effectively rendering the luminance distribution symmetric. (**c**) Luminance-remapped image set in which the luminance distribution of natural images was remapped onto phase-scrambled images. (**d**) Luminance-remapped image set in which the luminance distribution of phase-scrambled images was remapped onto natural images. Dots represent individual observations and black bars indicate group averages ($N = 50$ cross-validations for all image sets). No significance tests were performed in this figure.

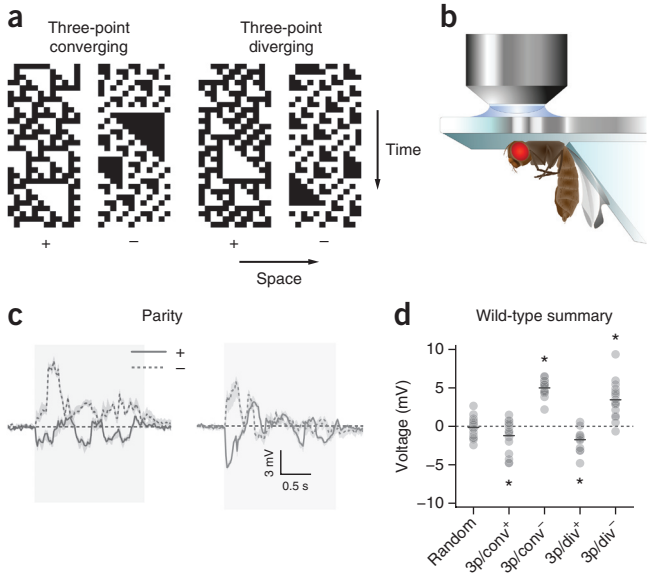


**Figure 7** LPTCs are sensitive to higher order correlation stimuli. (**a**) Space-time plots of glider stimuli used to probe LPTC sensitivity to triple correlations. (**b**) Schematic drawing of *in vivo* electrophysiology preparation and setup. (**c**) Average responses to full-field three-point glider stimulation of pooled vertical and horizontal system cells ($n = 16$ cells from $N = 12$ flies). Gray shaded area shows duration of stimulus presentation. Shaded areas surrounding traces signify bootstrapped 68% confidence intervals around the mean. (**d**) Quantification of integrated responses (averaged over the first second of stimulus presentation); "3p/conv" or "3p/div" indicate three-point converging or diverging glider orientation, respectively, and superscript the stimulus parity. All recordings were done in wild-type Canton S flies. Depicted responses are the difference between glider presentation in preferred and null direction. Dots represent individual observations and black bars show group averages. Asterisks indicate significant differences from zero after two-tailed *t* tests (*$P < 0.05$); exact test statistics are reported in **Supplementary Table 6**.

properties to diverge between ON and OFF channels. Finally, replacing the skewed luminance distribution of natural images with a symmetric one again abolished the temporal tuning differences (**Fig. 6d**). Notably, the DC asymmetry did not depend on higher order statistics of the stimulus. This particular tuning difference may be advantageous for ON-OFF detectors regardless of image statistics.

Taken together, our optimization findings demonstrate that, in realistic environments, the ON and OFF channels of motion detectors that were optimal under our criterion were tuned asymmetrically. The specific parameters that best estimated motion in natural scenes reproduced tuning properties of the biological fly motion detector we determined experimentally. At no point did we use our previous experimental findings as a constraint during optimization; the procedure arrived at this specific asymmetry independently.

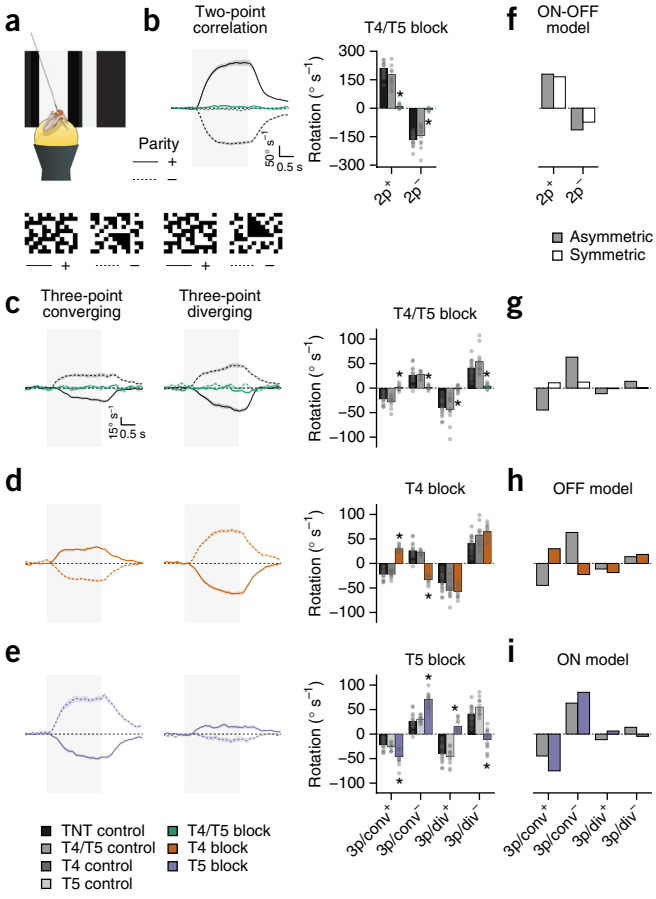


**Figure 8** Behavioral sensitivity to higher order correlations depends on T4 and T5 and is predicted by an asymmetric ON-OFF model. (**a**) Illustration of behavioral experiment. (**b**) Two-point glider responses. Left, average response traces for two-point glider stimuli. Here, as in all following panels, the gray shaded area indicates stimulus presentation. Right, rotational responses for two-point gliders representing phi and reverse-phi motion are abolished in T4/T5 block flies. (**c**) Control flies respond to three-point gliders in a specific pattern. Blocking T4 and T5 in conjunction eliminates these responses completely. (**d**,**e**) Silencing T4 or T5 modulates responses by reversing rotation for converging or diverging gliders, respectively. (**f**) Asymmetric and symmetric models account for two-point glider responses. (**g**) Only the asymmetric model correctly predicts three-point glider responses of control flies. (**h**,**i**) Simulating individual T4 and T5 blocks in the asymmetric ON-OFF model by setting the gain for either ON (red) or OFF (blue) channel to zero replicates the behavioral effects. Shaded areas surrounding traces signify bootstrapped 68% confidence intervals around the mean. Dots represent individual flies and bars show group averages. Asterisks indicate significant differences of block flies from both Gal4 and UAS controls after Bonferroni-corrected two-tailed *t* tests ($N = 18$ for TNT control, $N = 12$ for T4/T5 control, $N = 12$ for T4 control, $N = 12$ for T5 control, $N = 14$ for T4/T5 block, $N = 13$ for T4 block, $N = 17$ for T5 block; *$P < 0.05$). Exact test statistics are reported in **Supplementary Table 7**.

**Higher-order motion sensitivity derives from ON-OFF asymmetry**

Theoretical considerations indicate that spatiotemporal correlations of orders higher than two become informative indicators of visual motion in environments that are ON-OFF asymmetric[14]. Hassenstein-Reichardt detectors exclusively capture two-point correlations. Experimental work, however, confirmed that *Drosophila* responds to triple correlations[12]. This suggests that such correlations are either computed explicitly by secondary circuits or implicitly extracted by detectors that treat ON and OFF motion differentially. We assessed whether an asymmetric detector can account for *Drosophila*'s sensitivity to higher order motion.

First, we tested whether tangential cells respond to higher order motion cues given that these neurons receive their primary direction-selective input from T4 and T5 (ref. 30). We made use of previously characterized three-point glider stimuli[12,15] (**Fig. 7a**), which enforce the mean sign of correlations across three spatiotemporal points. They have four possible forms: converging or diverging, depending on their spatiotemporal orientation, and either positive or negative parity. Notably, they are guaranteed to contain on average zero

directed two-point correlations, allowing the isolated characterization of responses to higher order motion. When we recorded from tangential cells of both the horizontal and vertical system (**Fig. 7b**), they responded to single instantiations of three-point gliders with complex dynamics (**Fig. 7c**). Their time-averaged voltage signals replicated the response pattern observed for behaving flies[12] (**Fig. 7d**). Given that fly locomotion is thought to reflect integrated tangential cell responses[26], the combination of T4 and T5 thus appeared to be sufficient for higher order motion sensitivity.

We then examined the necessity of T4 and T5 for three-point glider responses. Tethered walking flies were presented with a complete set of two-point and three-point gliders (**Fig. 8a**). Next, we silenced T4 and T5 in isolation as well as simultaneously. For control flies, turning responses to two-point correlations were as expected for standard phi and reverse-phi stimuli: flies turned strongly in the direction of positive correlations (positive glider parity) and reversed this tendency for negative correlations (negative glider parity; **Fig. 8b**). Blocking T4 and T5 in conjunction completely abolished sensitivity to all two-point gliders. This is, to the best of our knowledge, the first demonstration that reverse-phi motion, defined by spatiotemporal anti-correlations, depends on the combined activity of ON and OFF motion detectors[10,19,36]. We then replicated the previously reported behavioral response pattern for three-point gliders[12]. Flies in which both T4 and T5 were silenced failed to respond to any of the higher order motion stimuli, indicating that T4 and T5 are also necessary for motion detection beyond two-point correlations (**Fig. 8c**). Blocking T4 or T5 in isolation had no effect on two-point responses (**Supplementary Fig. 6a–c**). We were, however, surprised to find that isolated T4 or T5 blocks resulted in particular three-point glider phenotypes. Silencing the ON pathway specifically reversed the flies' turning tendency for converging gliders while slightly boosting diverging glider responses (**Fig. 8d**). For OFF block flies, the opposite pattern emerged (**Fig. 8e**).

Finally, we probed our symmetric and asymmetric detector models for higher order motion sensitivity. Both produced comparable two-point glider responses (**Fig. 8f**). For three-point gliders, both detectors generated nonzero output, but only the asymmetric model qualitatively matched the pattern we observed in our electrophysiological experiments as well as in walking flies (**Fig. 8g**). Notably, when evaluating detector responses to individual glider instantiations, we found complex and strongly fluctuating responses that resembled tangential cell responses (**Supplementary Fig. 6d**,**g**). Responses became smooth and regular only after integration of many repetitions (**Fig. 7** and **Supplementary Fig. 6e**,**f**,**h**,**i**). We then simulated T4 or T5 silencing by setting ON or OFF gain to zero. These models reliably predicted the specific response reversals (**Fig. 8h**,**i**) observed in behavior (**Fig. 8d**,**e**). We therefore posit that T4 and T5 are capable of extracting triple correlations on their own. ON and OFF edges have been found to contain a particular combination of triple correlations[12]. The reverse also held: three-point gliders elicited strong signals of opposite sign in pure ON or OFF detectors (**Fig. 8d**,**e**,**h**,**i**). Only if the pathways were perfectly symmetric did these responses cancel out. If they were asymmetric, as in our optimized detector or the *Drosophila* visual system, then residual responses remained. Our optimized models correctly predicted the sign and relative magnitude of these effects, suggesting that the asymmetries we found *in silico* track the asymmetries of the biological system.

## DISCUSSION

We studied the roles of ON and OFF motion pathways for velocity estimation in natural scenes. *Drosophila* stabilized their walking trajectories in a closed-loop virtual environment whose statistics resembled those of natural scenes. Genetically silencing cells T4 and T5 rendered flies unable to perform this path correction. In an open-loop setting, flies reliably tracked whole-field motion of naturalistic images. Interrupting the activity of ON or OFF pathways did not affect this capability, suggesting that the two channels subserve redundant functions in information-rich natural scenes. In physiological and behavioral experiments, we found that ON and OFF motion estimators exhibit diverging temporal tuning. When we optimized the estimation performance of an ON-OFF motion detector, we obtained asymmetric models whose temporal tuning properties resembled those found for the biological system. This suggests that *Drosophila* motion detectors are tailored to an ON-OFF asymmetric visual world, with each channel covering the most informative temporal range. In a final set of experiments and without specific tuning of the model, we found that *Drosophila's* sensitivity to certain types of higher order motion has a straightforward explanation in this framework of differentially tuned pathways.

One could interpret the shifted tuning ranges of T4 and T5 as a solution for maximizing information transfer by avoiding coding redundancy. However, for the asymmetric detector, pathways were optimized independently, forcing both to adequately encode the input velocity distribution. We therefore favor the interpretation that features reliably indicating scene velocity operate on time scales that differ between ON and OFF signals. The skewed luminance distribution of real images (**Fig. 6a**) offers an intuition for this notion: ON signals are dominated by infrequent and large positive deflections, whereas OFF signals are generally smaller and more regular. As neither RC filters nor lamina cells act as perfect differentiators, these differences plausibly persist at later levels of motion detection, where they may be exploited by appropriately tuned mechanisms[13]. Notably, detector performance was generally better for OFF detectors than for ON detectors (**Fig. 5b**), possibly reflecting the sparseness of informative ON signals.

During conditioning of detector parameters on natural images, we also optimized the weight of the tonic DC signal. We found nonzero optima for both pathways, as postulated in previous studies on reverse-phi responses[10]. Electrophysiologically, ON pathway interneurons Mi1 and Tm3 did indeed show static responses to absolute brightness levels with the amplitude ratio between high-pass and DC signal qualitatively matching our findings[24]. In contrast to our prediction, OFF intermediaries Tm1 and Tm2 did not exhibit inverted tonic signals. However, other cells presynaptic to T5 still await characterization[17]. How DC signals can be reconciled with our demonstration that T4 and T5 responses are fully polarity specific remains unclear. In particular, theoretical considerations on the basis of the response properties of Mi1 and Tm3 predict sensitivity to OFF edges for T4 (ref. 24). This is not borne out by our experiments (**Fig. 3**).

Theoretical studies have proposed that responding to higher order correlations allows motion detectors to exploit natural ON-OFF asymmetries[12,14]. The asymmetry between ON and OFF pathways reported here does indeed confer sensitivity to triple correlations. Only under the assumption that ON and OFF steps are processed equally do spurious two-point correlations vanish. However, whether *Drosophila's* higher order motion responses are an epiphenomenon of detector asymmetries or whether detector asymmetry represents a way of accessing higher order correlations is up for debate. Moreover, it remains to be seen whether the findings at hand generalize to other forms of higher order motion perceived by *Drosophila*[38].

Our previous characterization of cell types T4 and T5 revealed only minor differences in temporal frequency tuning for gratings[21]. It is currently not well understood how physiological tuning curves for edges and gratings relate to each other. Given the drastically different

kinetics of the two stimuli, large ON-OFF differences for one may lead to only small ON-OFF differences for the other. In addition, we suggest that edges provide a better approximation of visual kinetics in the real world than artificial gratings that are periodic as well as constant in mean luminance, contrast and geometry. Moreover, measurements from tangential cells in behaving flies have indicated grating response optima that are shifted toward higher frequencies compared with quiescence[26,39,40]. How this state dependency translates to the tuning for edge velocity is unclear. Indeed, our linear prediction of opposing edge responses from physiological edge tuning underestimates the true crossing point between ON and OFF dominance (**Fig. 4d**). A shift toward higher preferred velocities, as observed for grating optima, could account for this discrepancy. Notably, our behavioral data demonstrate that basic characteristics of temporal ON-OFF asymmetries are preserved in active flies.

The ON-OFF asymmetry we describe represents one of many examples for the adaptation of sensory systems to the environment in which they evolved[5,6,13,41]. Contrast asymmetries between ON and OFF are a widespread feature shared by most visual niches. It therefore seems probable that the sensory asymmetries found in *Drosophila* are conserved across species. ON-OFF divergence has previously been described for several computations in vertebrate visual systems[42–44]. It will be interesting to examine the effects on optimal tuning exerted by features of the mammalian retina, such as contrast normalization[45]. Finally, motion energy models have been successfully used to explain the psychophysics of motion perception in higher organisms[46]. Given that Hassenstein-Reichardt detectors and motion energy models are generally mathematically equivalent[47], our optimization results could also emerge for an appropriately rectified ON-OFF motion energy detector.

T4 and T5 are critically involved in behaviors other than the optomotor response. Recently, studies have implicated motion detectors in object fixation[27], depth perception[48] or looming responses[49]. Given the variety of tasks and resulting visual statistics, optimal tuning needs to be examined under various constraints. Finally, we believe this ecological perspective on biological motion detection could have a decisive role in the continued mapping of the fly visual system. The abundance of information-bearing features in natural visual scenes may necessitate complex filter banks and multi-cell processing stages[17,20,23,50]. Real-world demands will then be critical constraints when assigning function to cells in the *Drosophila* optic lobe.

## METHODS

Methods and any associated references are available in the online version of the paper.

*Note: Any Supplementary Information and Source Data files are available in the online version of the paper.*

### ACKNOWLEDGMENTS

A. Nern and G.M. Rubin (Janelia Research Campus) generated and kindly provided the splitGal4 line targeting T4 and T5. We are grateful for fly work and behavioral experiments performed by R. Kutlesa, C. Theile and W. Essbauer. We thank A. Arenz and A. Mauss for carefully reading the manuscript, T. Schilling for fly illustrations, and all of the members of the Borst laboratory for extensive discussions. The Bernstein Center for Computational Neuroscience Munich supplied computing resources for our simulations. A.L., G.A., M.M., E.S., A. Bahl and A. Borst are members of the Graduate School for Systemic Neurosciences, Munich.

### AUTHOR CONTRIBUTIONS

A.L., G.A. and A. Borst designed the study. A.L. performed behavioral experiments, associated data analysis and all modeling work. G.A., M.M. and E.S. performed electrophysiological experiments. G.A. performed calcium imaging. A.L. and G.A. analyzed physiological data. A. Bahl designed the behavioral apparatuses and performed behavioral experiments. A.L. wrote the manuscript with help from all of the authors.

### COMPETING FINANCIAL INTERESTS

The authors declare no competing financial interests.



1. Borst, A. Fly visual course control: behavior, algorithms and circuits. *Nat. Rev. Neurosci.* **15**, 590–599 (2014).
2. Ruderman, D.L. & Bialek, W. Statistics of natural images: Scaling in the woods. *Phys. Rev. Lett.* **73**, 814–817 (1994).
3. Simoncelli, E.P. & Olshausen, B.A. Natural image statistics and neural representation. *Annu. Rev. Neurosci.* **24**, 1193–1216 (2001).
4. Field, D.J. Relations between the statistics of natural images and the response properties of cortical cells. *J. Opt. Soc. Am. A* **4**, 2379–2394 (1987).
5. Laughlin, S. A simple coding procedure enhances a neuron's information capacity. *Z. Naturforsch. C* **36**, 910–912 (1981).
6. van Hateren, J.H. & van der Schaaf, A. Independent component filters of natural images compared with simple cells in primary visual cortex. *Proc. Biol. Sci.* **265**, 359–366 (1998).
7. Yu, Y., Schmid, A.M. & Victor, J.D. Visual processing of informative multipoint correlations arises primarily in V2. *eLife* **4**, e06604 (2015).
8. Gjorgjieva, J., Sompolinsky, H. & Meister, M. Benefits of pathway splitting in sensory coding. *J. Neurosci.* **34**, 12127–12144 (2014).
9. Borst, A. & Helmstaedter, M. Common circuit design in fly and mammalian motion vision. *Nat. Neurosci.* **18**, 1067–1076 (2015).
10. Eichner, H., Joesch, M., Schnell, B., Reiff, D.F. & Borst, A. Internal structure of the fly elementary motion detector. *Neuron* **70**, 1155–1164 (2011).
11. Hassenstein, B. & Reichardt, W. Systemtheoretische Analyse der Zeit-, Reihenfolgen- und Vorzeichenauswertung bei der Bewegungsperzeption des Rüsselkäfers *Chlorophanus*. *Z. Naturforsch. B* **11**, 513–524 (1956).
12. Clark, D.A. *et al.* Flies and humans share a motion estimation strategy that exploits natural scene statistics. *Nat. Neurosci.* **17**, 296–303 (2014).
13. Ratliff, C.P., Borghuis, B.G., Kao, Y.-H., Sterling, P. & Balasubramanian, V. Retina is structured to process an excess of darkness in natural scenes. *Proc. Natl. Acad. Sci. USA* **107**, 17368–17373 (2010).
14. Fitzgerald, J.E., Katsov, A.Y., Clandinin, T.R. & Schnitzer, M.J. Symmetries in stimulus statistics shape the form of visual motion estimators. *Proc. Natl. Acad. Sci. USA* **108**, 12909–12914 (2011).
15. Hu, Q. & Victor, J.D. A set of high-order spatiotemporal stimuli that elicit motion and reverse-phi percepts. *J. Vis.* **10**, 9.1–9.16 (2010).
16. Takemura, S.-Y. *et al.* A visual motion detection circuit suggested by *Drosophila* connectomics. *Nature* **500**, 175–181 (2013).
17. Shinomiya, K. *et al.* Candidate neural substrates for off-edge motion detection in *Drosophila*. *Curr. Biol.* **24**, 1062–1070 (2014).
18. Joesch, M., Schnell, B., Raghu, S.V., Reiff, D.F. & Borst, A. ON and OFF pathways in *Drosophila* motion vision. *Nature* **468**, 300–304 (2010).
19. Clark, D.A., Bursztyn, L., Horowitz, M.A., Schnitzer, M.J. & Clandinin, T.R. Defining the computational structure of the motion detector in *Drosophila*. *Neuron* **70**, 1165–1177 (2011).
20. Silies, M. *et al.* Modular use of peripheral input channels tunes motion-detecting circuitry. *Neuron* **79**, 111–127 (2013).
21. Maisak, M.S. *et al.* A directional tuning map of *Drosophila* elementary motion detectors. *Nature* **500**, 212–216 (2013).
22. Meier, M. *et al.* Neural circuit components of the *Drosophila* OFF motion vision pathway. *Curr. Biol.* **24**, 385–392 (2014).
23. Ammer, G., Leonhardt, A., Bahl, A., Dickson, B.J. & Borst, A. Functional specialization of neural input elements to the *Drosophila* ON motion detector. *Curr. Biol.* **25**, 2247–2253 (2015).
24. Behnia, R., Clark, D.A., Carter, A.G., Clandinin, T.R. & Desplan, C. Processing properties of ON and OFF pathways for *Drosophila* motion detection. *Nature* **512**, 427–430 (2014).
25. Haikala, V., Joesch, M., Borst, A. & Mauss, A.S. Optogenetic control of fly optomotor responses. *J. Neurosci.* **33**, 13927–13934 (2013).
26. Schnell, B., Weir, P.T., Roth, E., Fairhall, A.L. & Dickinson, M.H. Cellular mechanisms for integral feedback in visually guided behavior. *Proc. Natl. Acad. Sci. USA* **111**, 5700–5705 (2014).
27. Bahl, A., Ammer, G., Schilling, T. & Borst, A. Object tracking in motion-blind flies. *Nat. Neurosci.* **16**, 730–738 (2013).
28. Joesch, M., Plett, J., Borst, A. & Reiff, D.F. Response properties of motion-sensitive visual interneurons in the lobula plate of *Drosophila melanogaster*. *Curr. Biol.* **18**, 368–374 (2008).
29. Warzecha, A.-K. & Egelhaaf, M. Intrinsic properties of biological motion detectors prevent the optomotor control system from getting unstable. *Phil. Trans. R. Soc. Lond. B* **351**, 1579–1591 (1996).
30. Schnell, B., Raghu, S.V., Nern, A. & Borst, A. Columnar cells necessary for motion responses of wide-field visual interneurons in *Drosophila*. *J. Comp. Physiol. A Neuroethol. Sens. Neural Behav. Physiol.* **198**, 389–395 (2012).

31. Brand, A.H. & Perrimon, N. Targeted gene expression as a means of altering cell fates and generating dominant phenotypes. *Development* **118**, 401–415 (1993).
32. Sweeney, S.T., Broadie, K., Keane, J., Niemann, H. & O'Kane, C.J. Targeted expression of tetanus toxin light chain in *Drosophila* specifically eliminates synaptic transmission and causes behavioral defects. *Neuron* **14**, 341–351 (1995).
33. Straw, A.D., Rainsford, T. & O'Carroll, D.C. Contrast sensitivity of insect motion detectors to natural images. *J. Vis.* **8**, 32.1–32.9 (2008).
34. Chen, T.-W. *et al.* Ultrasensitive fluorescent proteins for imaging neuronal activity. *Nature* **499**, 295–300 (2013).
35. Mauss, A.S. *et al.* Neural circuit to integrate opposing motions in the visual field. *Cell* **162**, 351–362 (2015).
36. Tuthill, J.C., Chiappe, M.E. & Reiser, M.B. Neural correlates of illusory motion perception in *Drosophila*. *Proc. Natl. Acad. Sci. USA* **108**, 9685–9690 (2011).
37. Dror, R.O., O'Carroll, D.C. & Laughlin, S.B. Accuracy of velocity estimation by Reichardt correlators. *J. Opt. Soc. Am. A Opt. Image Sci. Vis.* **18**, 241–252 (2001).
38. Theobald, J.C., Duistermars, B.J., Ringach, D.L. & Frye, M.A. Flies see second-order motion. *Curr. Biol.* **18**, R464–R465 (2008).
39. Jung, S.N., Borst, A. & Haag, J. Flight activity alters velocity tuning of fly motion-sensitive neurons. *J. Neurosci.* **31**, 9231–9237 (2011).
40. Chiappe, M.E., Seelig, J.D., Reiser, M.B. & Jayaraman, V. Walking modulates speed sensitivity in *Drosophila* motion vision. *Curr. Biol.* **20**, 1470–1475 (2010).
41. Dyakova, O., Lee, Y.-J., Longden, K.D., Kiselev, V.G. & Nordström, K. A higher order visual neuron tuned to the spatial amplitude spectra of natural scenes. *Nat. Commun.* **6**, 8522 (2015).
42. Komban, S.J. *et al.* Neuronal and perceptual differences in the temporal processing of darks and lights. *Neuron* **82**, 224–234 (2014).
43. Chichilnisky, E.J. & Kalmar, R.S. Functional asymmetries in ON and OFF ganglion cells of primate retina. *J. Neurosci.* **22**, 2737–2747 (2002).
44. Pandarinath, C., Victor, J.D. & Nirenberg, S. Symmetry breakdown in the ON and OFF pathways of the retina at night: functional implications. *J. Neurosci.* **30**, 10006–10014 (2010).
45. Carandini, M. & Heeger, D.J. Normalization as a canonical neural computation. *Nat. Rev. Neurosci.* **13**, 51–62 (2012).
46. Adelson, E.H. & Bergen, J.R. Spatiotemporal energy models for the perception of motion. *J. Opt. Soc. Am. A* **2**, 284–299 (1985).
47. van Santen, J.P. & Sperling, G. Elaborated Reichardt detectors. *J. Opt. Soc. Am. A* **2**, 300–321 (1985).
48. Schwegmann, A., Lindemann, J.P. & Egelhaaf, M. Depth information in natural environments derived from optic flow by insect motion detection system: a model analysis. *Front. Comput. Neurosci.* **8**, 83 (2014).
49. Schilling, T. & Borst, A. Local motion detectors are required for the computation of expansion flow-fields. *Biol. Open* **4**, 1105–1108 (2015).
50. Burge, J. & Geisler, W.S. Optimal speed estimation in natural image movies predicts human performance. *Nat. Commun.* **6**, 7900 (2015).

## ONLINE METHODS

**Fly strains** and **genetics.** We raised *Drosophila melanogaster* on cornmeal-agar medium under standard conditions (60% humidity, 18 °C for behavioral and 25 °C for physiology experiments, 12-h light/12-h dark schedule) for the full duration of their developmental cycle. Female flies were used in all experiments. For physiological experiments, we selected flies 5–20 h post-eclosion. Flies in behavioral experiments were 1–3 d old. Behavioral experiments targeting T4 or T5 used the following driver lines, as described previously[21]: T4-Gal4 (VT37588) and T5-Gal4 (R42H07). When targeting T4 and T5 simultaneously, we employed a new, highly specific driver line: T4/T5-splitGal4 (R59E08-AD; R42F06-DBD), kindly provided to us by A. Nern and G.M. Rubin at Janelia Research Campus. For visualization of expression patterns (**Supplementary Fig. 1**), we crossed driver lines to UAS-mCD8GFP reporter flies. For experiments, Gal4 flies were then crossed to either wild type Canton S flies or UAS-TNT-E flies resulting in Gal4 control or block flies, respectively. Crossing UAS-TNT-E flies to Canton S flies generated UAS control flies. For calcium imaging, we combined two different Gal4 lines (VT25965 and VT37588) that in conjunction expressed at comparable levels in T4 and T5. These were crossed to UAS-GCaMP6f[34] flies. Genotypes derived from these crossings and their aliases as used throughout the text are listed in the supplementary material (**Supplementary Table 1**).

**Immunohistochemistry.** Antibody stainings (**Supplementary Fig. 1**) were performed as described previously[51]. We used the following antibodies and dilutions. Primary antibodies: rabbit anti-GFP (Torri Pines, TP401, 1:2,000), mouse anti-nc82 (DSHB, AB_2314866, 1:25); secondary antibodies: goat anti-rabbit 488 (Invitrogen, A-11008, 1:500), goat anti-mouse 633 (Invitrogen, A-21053, 1:500). Imaging was performed on a SP5 confocal microscope (Leica) at a resolution of 1,024 × 1,024. Images were processed in ImageJ 1.46f (US National Institutes of Health). Single z-slices are shown for horizontal views.

**Behavioral experiments.** We performed behavioral experiments as described previously[21,23,27]. Briefly, tethered flies were placed on an air-suspended polyurethane ball in a virtual environment consisting of three computer screens covering a substantial part of the animal's visual field (approximately 270° in azimuth and 120° in elevation). Experiments were run on six set-ups in parallel; two of them displayed visual stimuli at 120 Hz and the remaining four at 144 Hz with all screens calibrated to display at comparable contrast and brightness. We never observed any differences in behavior between refresh rates. All stimuli were rendered in real-time using the graphics engine Panda3D, allowing visual feedback based on flies' instantaneous walking behavior. Due to high pixel density on all computer screens, stimulus pixel size was well below the resolution limit of *Drosophila*. The immediate surround of the ball was temperature-controlled by means of a closed-loop thermoregulation system. Each experiment used the same temperature protocol: Temperature was kept at 25 °C for the first 5 min and then linearly raised to 34 °C within 10 min.

All behavioral experiments ran for 60–90 min and comprised 50–60 repeated trials, except for open-loop velocity estimation experiments (**Fig. 2**) that lasted 280 trials. In each trial, we randomized stimulus presentation order. Movement of the ball was tracked at 4 kHz and down-sampled to 20 Hz for offline analysis. For each fly, we manually selected a continuous range of 100–200 (**Fig. 2**) or 25 trials (other experiments) based on the following criteria: First, the temperature was at a constant 34 °C. Second, the average forward walking speed of the fly was above 0.3 cm $s^{-1}$, indicating healthy locomotion and visual responsiveness. Third, the average turning tendency of the fly was stable and close to 0° $s^{-1}$. These criteria excluded approximately 20% of all flies we measured. During analysis, we averaged traces across trials, resulting in a single walking trace per fly per experimental condition. Where applicable (**Figs. 1**, **4** and **8**, and **Supplementary Fig. 5**), we then subtracted responses to mirror-symmetric stimulus presentations to minimize the impact of small rotational biases in turning behavior. Traces were filtered using a first-order low-pass filter ($\tau$ = 100 ms). In open-loop experiments (**Fig. 2**), we generated a regression model for each fly that mapped rotation of the environment to the turning response of the fly (averaged over 1 s after stimulus onset) using least-squares fitting. Response gain was then defined as the slope of this model. The intercepts clustered around 0° $s^{-1}$, indicating trajectories that were on average straight. For additional analysis (**Supplementary Fig. 3**), we constructed Bayesian decoders that minimize the squared error of their estimates. This was done on a fly-by-fly basis. We first split the data set consisting of pairs of image velocity and turning response as for the correlation analysis (**Fig. 2**) into training and test sets at a ratio of 3:1, approximated the posterior distribution through application of Bayes' rule to the joint probability generated from appropriate histograms, and estimated image velocity as the expected value of the posterior for a given response. Finally, we assessed decoding performance of resulting mapping functions by calculating the root-mean-square error after application to the test set. The behavioral data analysis pipeline was implemented in Python 2.7 using pandas 15.1, NumPy 1.6, SciPy 0.15, matplotlib 1.3 and Numba 0.18.

**Electrophysiology.** Electrophysiological *in vivo* patch-clamp recordings from lobula plate tangential cells closely followed previously described protocols[21,22,28]. Recordings were low-pass filtered with a cut-off frequency of 3 kHz and digitized at 10 kHz. Data acquisition was based on Matlab R2011A (MathWorks). We identified cell types based on their response profile when stimulated with moving gratings. In addition, cells were dye-filled and anatomically verified whenever possible.

We visually stimulated flies using a custom-built LED arena spanning approximately 180° in azimuth and 90° in elevation of the fly's visual field with a spatial resolution of 1.5° per individual LED. The LED refresh rate was in the kHz range; stimulus images were then updated with up to 600 Hz. Maximum luminance was 80 cd $m^{-2}$. During offline data analysis, recorded traces were down-sampled to 2 kHz and averaged across 2–5 trials per cell. We randomized the order of stimulus presentation within trials. Cells that did not respond reliably to grating stimulation were excluded from further analysis. Before we extracted response maxima and minima for edge responses (**Fig. 3**), electrophysiological traces were filtered with a second-order Savitzky-Golay kernel that was 40 samples wide. The electrophysiological data analysis pipeline was implemented in Python 2.7 using pandas 15.1, NumPy 1.6, matplotlib 1.3 and Numba 0.18.

**Calcium imaging.** We employed a custom-built two-photon laser scanning microscope as described previously[21,22]. We prepared flies analogously to electrophysiology experiments. Images were recorded at a resolution of 256 × 128 pixels and a frame rate of 3.74 Hz. Raw images were then converted into relative fluorescence change ($\Delta F/F$) series by using the mean of three frames before stimulation onset as a baseline. For summary images, the resulting images were averaged across time; for time-resolved traces, we defined relevant regions of interest and collapsed signals within the defined borders by averaging across pixels. We used the LED arena described above for visual stimulation. Data acquisition and analysis were performed in Matlab R2011a (MathWorks) using ScanImage 3.8.

**Image sets.** Two image sets were used throughout the study. First, for all behavioral experiments involving natural images, we generated a small library of 60 panoramic images spanning approximately 360° in azimuth using a consumer-grade camera (iPhone 5s; Apple). The resolution of each image was 10,800 × 2,460 pixels. Images were taken in various natural environments covering different visual statistics: woods (30%), open rural spaces (30%), urban landscapes (20%), and laboratories (20%). We used raw images without processing or calibration and converted them to gray scale by averaging across color channels. Critical image statistics such as RMS contrast (that is, the s.d. of pixel values), luminance distribution, and power spectrum were comparable to other scientific image libraries. Second, for all *in silico* experiments, we made use of calibrated images from the van Hateren natural image database[6]. No image category was excluded and we performed no further sorting, yielding 4,167 images at a resolution of 1,536 × 1,024 pixels. One pixel corresponded to one arc minute of visual angle. We normalized the set through subtraction of and division by the mean pixel value for each image[12,45]. Kernel density estimates (**Figs. 2** and **6**) were generated using a routine in the SciPy library. Gaussian kernels were used, and we determined bandwidth via Silverman's rule.

We scaled the contrast of our in-house image set by subtracting the image's mean luminance, applying the specified multiplicative factor, and then adding the initial mean luminance (**Figs. 1** and **2**). Phase-scrambling of the van Hateren image set was achieved by performing a Fourier transform, replacing the phase spectrum with that of a Gaussian random image of equal mean luminance, and finally recovering the phase-randomized image via the inverse Fourier transform (**Fig. 6b**). The luminance-remapped scrambled set was generated by replacing each pixel value of a phase-randomized image with the value corresponding to

the same luminance-ordered rank in the original image (**Fig. 6c**). Analogously, we generated the luminance-remapped natural set by drawing pixel values from the corresponding phase-scrambled image (**Fig. 6d**).

**Visual stimuli.** On every trial of the closed-loop course stabilization experiment (**Fig. 1**), a random image was chosen from our in-house image library and projected onto a virtual cylinder surrounding the fly. In order to cover the visual field without significant distortion, the panorama was mirrored across the fly's elevation axis. Each trial lasted 5 s. The rotational component of the walking trajectory was used as a feedback signal for the azimuthal orientation of the virtual cylinder, effectively giving flies control over their angular orientation relative to the environment. Feedback gain was set to unity. Between 1.5 s and 3.5 s, we additionally rotated the virtual environment at a constant 80° $s^{-1}$ in clockwise or counter-clockwise direction. Contrast was scaled in accordance with the procedure described above to 12.5%, 25%, 50% and 100% of the original RMS value.

For open-loop velocity estimation experiments (**Fig. 2**), images were chosen and projected as above while feedback gain was set to zero. On each trial, a random velocity was drawn from a Gaussian distribution centered at 0° $s^{-1}$ with a s.d. of 50° $s^{-1}$. Trials lasted 3.5 s. Between 1.5 s and 2 s, the virtual environment rotated with the constant velocity drawn earlier. The border where the image on the cylinder wrapped around was placed such that it remained in the back of the fly on most trials. Here, we added the 6% contrast condition.

We used single bright and dark edges for characterizing the physiological response properties of ON and OFF channels (**Fig. 3**). During electrophysiology experiments, we presented edges moving at 12 constant velocities across two orders of magnitude (6.25, 12.5, 25, 50, 75, 100, 150, 200, 300, 500, 700 and 900° $s^{-1}$). When recording from vertical system or horizontal system cells, edges traveled along the vertical or horizontal axis, respectively, and in the preferred direction of the cell. Edges used during calcium imaging always moved at 25° $s^{-1}$ and either downwards or from front to back (no differences between the two directions were observed). Physiology stimuli (**Fig. 3**) had a Michelson contrast of 100%, starting from either a dark (ON) or bright (OFF) background. For additional experiments (**Supplementary Fig. 4**), edges started from an equal background luminance of 10.7 cd $m^{-2}$. As the stimulation device only allowed discrete steps, ON edges then had a contrast of 76% and OFF edges a contrast of 100%.

The behavioral balanced motion stimulus resembled previous iterations[19,21,23]. Briefly, we presented flies with a stationary square wave grating that had an initial spatial wavelength of 45° and Michelson contrast of 50%. Each individual trial lasted 9 s. Between 2 s and 7 s, bright and dark edges moved in opposite directions at the same velocity. In contradistinction to previous experiments, we reset the stimulus to the initial state after edges had traversed 20° of visual angle, allowing us to keep stimulus duration fixed regardless of edge velocity. After each reset, we applied a random phase shift in order to minimize the effect of initial grating position relative to the fly. This was done for six velocities (20, 40, 80, 160, 320 and 640° $s^{-1}$) in clockwise and counter-clockwise direction. Pulse experiments (**Supplementary Fig. 5**) were performed analogously, with edge movement being limited to the indicated duration (500 ms, 250 ms or 100 ms).

Glider experiments (**Figs. 7** and **8**) were performed as described previously[12]. Briefly, the visual field was divided into vertical stripes that had an azimuthal extent of 6° (behavior) or 4.5° (electrophysiology). Each bar could either be dark or bright; Michelson contrast for these experiments was 50% (behavior) or 100% (electrophysiology). Initial bars were seeded with a random binary pattern. Depending on the glider, bars were then updated according to the corresponding deterministic rule. The glider update frequency was either 24 Hz (behavior) or 10 Hz (electrophysiology). For electrophysiological experiments, we used a single pre-generated glider sequence. Here, preferred direction was defined as the update direction that would depolarize cells for two-point gliders.

**Modeling.** The ON-OFF detector used in this study (**Figs. 5**, **6** and **8**) was derived from a previously published two-quadrant model[10]. Briefly, we modeled photoreceptor signals as time series with a resolution of 10 ms (for optimization experiments) or 1 ms (for other experiments) per step. Lamina processing was then approximated as the linear sum of a high-pass-filtered signal (first-order RC filter with $\tau = 250$ ms) and an unfiltered tonic component (DC) with variable weight. This was followed by a half-wave rectification step. For the pure ON detector, signals were rectified with the threshold set to exactly zero. For the pure OFF detector, the signal was inverted and then rectified with the threshold set to exactly zero. Further processing was identical for both: The signal was first-order low-pass filtered with variable time constant $\tau$ and then multiplied with an unfiltered signal from the other spatial location. This was done twice in a mirror-symmetrical fashion, followed by subtraction, yielding a fully opponent direction-selective signal. For the full ON-OFF detector, an ON detector and an OFF detector were summed with equal weight. Unlike previous versions[10], our simplified detector did not make use of shifted rectification thresholds or unequally weighted detector halves. Outside of natural image experiments, stimuli were rendered at a spatial resolution of 0.1°. We modeled the spatial acceptance profile of photoreceptors as Gaussians with a half-width at maximum of 5°. The symmetric detectors (**Figs. 5** and **8**) had, by definition, zero DC component and identical filter time constants for the ON and the OFF channel as determined by the optimization procedure. The asymmetric detector had DC components and time constants that were allowed to differ between ON and OFF during optimization.

The detector characterization (**Fig. 5**) depicts results from a combination of 20 detectors separated by 6.5°. The spatial wavelength of all gratings was 20° with velocity being defined by temporal frequency. Simulations for grating and edge tunings ran for 10 s each; output was averaged across detectors and time. For the velocity profile (**Fig. 5g**), we used a time series drawn from a Gaussian distribution with s.d. = 20° $s^{-1}$ that was first-order low-pass filtered with $\tau = 500$ ms. Units were discarded for display purposes. Modeled edge stimuli lasted for 15 s, with movement starting after 2 s. The starting condition was fixed at 1.0 and followed by a jump to 1.2 for ON edges or 0.8 for OFF edges. Detector output was averaged for the duration of edge motion, which depended on velocity. We simulated 50 velocities on a logarithmic scale from 10° $s^{-1}$ to 1,000° $s^{-1}$. Glider stimuli (**Fig. 8**) were rendered as idealized signals mapping 21 virtual stripes to the 21 virtual photoreceptors of an array of 20 detectors, without any spatial overlap. The array was seeded with a random combination of binary dark and bright values (arbitrarily defined as 1.0 and 3.0, respectively) and then updated according to previously described rules[12] at a frequency of 5 Hz. Glider simulations ran for 5 s each and were averaged across 500 instantiations and time (**Fig. 8f–i**). We approximated compressive characteristics of the visuo-motor transformation by multiplying two-point and three-point responses with slightly different gain values (2,500° $s^{-1}$ and 3,500° $s^{-1}$, respectively) when translating detector output into turning tendency. All simulations were implemented in Python 2.7 using NumPy 1.6 and Numba 0.18.

**Detector optimization.** Optimization of detector models was based on an exhaustive cross-validated search on a two-dimensional parameter grid. We generated 50 random training-to-test splits from the 4,167 images of the van Hateren data set with a training-to-test ratio of 4:1. All images received a luminance bias of 3.0 and were clipped at zero in order to ensure that only positive signals arrived at detector inputs while keeping mean values constant. The optimization procedure was then performed independently for each training fold.

We scanned a parameter space comprising 40 × 21 combinations of low-pass time constants (from 10 to 400 ms in 10-ms steps) and DC contribution (from −20% to +20% in 2% steps). For each parameter set, three detectors with the corresponding parameter settings were simulated: a pure ON detector, a pure OFF detector, and a symmetric ON-OFF detector where ON and OFF channels used the same parameters. Fitness of a given detector was determined as follows, based on previous studies[12] and analogously to behavioral experiments (**Fig. 2**): on each iteration, we drew a random image from the training set and a random velocity from a Gaussian distribution centered at zero with s.d. = 25° $s^{-1}$. We then generated two time series corresponding to a simulated pair of photoreceptors separated by 6.5° traveling across the horizontal middle row of the image at the constant velocity drawn before and for a duration of 1,000 ms. The signals were fed into each of the three detectors. Detector output was averaged across time. We repeated this procedure 50,000 times per parameter set. Detector fitness was then defined as the Pearson correlation between input velocity and average detector output. During testing, we assembled two detectors per test set. The optimal symmetric detector was the best-performing detector constrained to use equal ON and OFF settings and zero DC. The optimal asymmetric detector was the linear combination of the best performing ON detector and the best performing OFF detector. The performance of both was then evaluated on the corresponding test set; here, detector evaluations were repeated 100,000 times. This was done for the natural, phase-scrambled and luminance-remapped image sets.




doi:10.1038/nn.4262

We implemented the optimization procedure in Python 2.7 using NumPy 1.6, SciPy 0.15, Numba 0.18, and IPython 3.0. Parallel operations were distributed across 128 CPUs on a Beowulf cluster consisting of eight physical machines.

**Code availability.** Python and Matlab code used throughout analysis, modeling, and optimization is available upon request to the authors.

**Statistics.** All statistical tests were two-tailed Student's *t* tests at a significance level of 0.05, assuming unequal variance unless stated otherwise. Where necessary, conservative Bonferroni correction was applied in order to correct for multiple hypothesis testing. Normality of data was confirmed visually and not formally tested. We did not predetermine sample sizes using statistical tests, but numbers are in line with established work[12,20,21,23,27]. Our confidence intervals were computed according to a bootstrapping procedure based on 1,000 re-samplings of the data set. We did not differentiate levels of significance; only single asterisks are used regardless of *P* value. Statistical procedures were used as implemented in SciPy 0.15. All experiments and data analysis were performed without blinding to conditions or genotypes.

A **Supplementary Methods Checklist** is available.

51. Yu, J.Y., Kanai, M.I., Demir, E., Jefferis, G.S.X.E. & Dickson, B.J. Cellular organization of the neural circuit that drives *Drosophila* courtship behavior. *Curr. Biol.* **20**, 1602–1614 (2010).

# Erratum: Asymmetry of *Drosophila* ON and OFF motion detectors enhances real-world velocity estimation

**Aljoscha Leonhardt, Georg Ammer, Matthias Meier, Etienne Serbe, Armin Bahl & Alexander Borst**
***Nat. Neurosci.*; doi:10.1038/nn.4262; corrected online 7 March 2016**

In the version of this article initially published online, the second and third authors of ref. 40, J.D. Seelig and M.B. Reiser, were replaced by the second author of ref. 39, A. Borst. The error has been corrected for the print, PDF and HTML versions of this article.